PAPER

Superparamagnetism in iron-doped CeO_{2-y} nanocrystals

J. Phys.: Condens. Matter **24** (2012) 456001 (6pp) doi:10.1088/0953-8984/24/45/456001

Superparamagnetism in iron-doped CeO_{2-y} nanocrystals

N Paunović, Z V Popović and Z D Dohčević-Mitrović

Center for Solid State Physics and New Materials, Institute of Physics, University of Belgrade, Pregrevica 118, 11080 Belgrade, Serbia

E-mail: zoran.popovic@ipb.ac.rs

Received 29 August 2012, in final form 28 September 2012
Published 17 October 2012
Online at stacks.iop.org/JPhysCM/24/456001

Abstract

We have measured the magnetization of undoped and $Fe^{2+/3+}$ doped CeO_{2-y} nanocrystals at various temperatures and magnetic fields. The Stoner condition $N(0)I > 1$ is multiply fulfilled in the case of nano-CeO_{2-y}, favoring the band ferromagnetism approach. In the case of Fe-doped samples, the magnetization versus magnetic field dependence is well fitted with a weighted Langevin function. A blocking temperature of about 20 K is obtained both from the ZFC/FC curves and from the coercive field against temperature dependence. The temperature and field dependence of the magnetization clearly shows the presence of nanosized particles which exhibit superparamagnetic behavior.

(Some figures may appear in colour only in the online journal)

1. Introduction

The magnetic properties of materials fundamentally change when the particle sizes are reduced [1]. Below a critical size (D_C), which typically lies below 100 nm, normal microscopic multidomain ferromagnetic (FM) structure is energetically unfavorable, and the particles are in the single domain state, figure 1. In this state, the mechanism of magnetization reversal can only occur via the rotation of the magnetization vector from one easy magnetic direction to another over the magnetic anisotropy barrier. The magnetic properties of the single domain state were analyzed in a seminal work first published by Stoner and Wohlfarth [2]. As particle size decreases within the single domain range, another critical threshold (D_{SP}) is reached, at which remanence and coercivity go to zero and the particles are in the superparamagnetic (SP) state. Such a system has no hysteresis and magnetization curves at different temperatures superimpose onto a universal curve of M/M_S versus H/T (Langevin's curve). A schematic representation of the coercivity change versus particle size is given in figure 1. The finite size effects in magnetic nanooxides [3] and magnetic rare-earth semiconducting materials [4, 5] have recently been a subject of great interest.

The appearance of the room temperature ferromagnetism in many oxide nanomaterials is related to oxygen vacancies [6], which play a crucial role in changing the electronic structure of oxides on the nanoscale and causing pronounced change in magnetic properties. The ferromagnetism in ceria thin films and nanoparticles has been found in pure samples and samples doped with 3d and 4f elements [7–11].

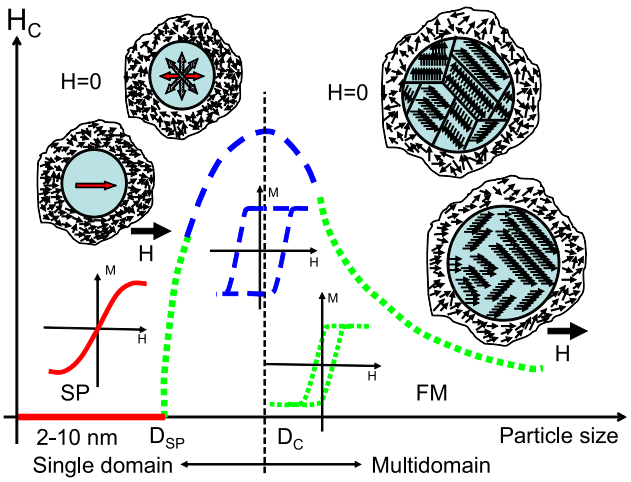

Figure 1. Schematic representation of the coercivity change as a function of particle size in an ultrafine particle system. The hysteresis loops of superparamagnetic (SP) and ferromagnetic (FM) states are also shown. D_C—critical size of multidomain (MD)/single domain (SD) transition; D_{SP}—critical particle size of FM/SP transition.

There are two different approaches for the explanation of the ferromagnetism in ceria oxide.

(i) The Heisenberg approach, where ions have certain localized magnetic moment, which interacts with the magnetic moment of the neighbors through an exchange coupling J. This approach was used by Han *et al* [12] to explain ferromagnetism in cerium oxide. In the oxygen deficient CeO_{2-y}, two reduced Ce ions form a Ce–O–Ce bond with their neighboring oxygen anion, where the $Ce4f_{xyz}$–O2p–$Ce4f_{xyz}$ interaction is responsible for the magnetic properties. Because a Ce–O–Ce bond angle is close to 90°, according to the Goodenough–Kanamori–Anderson rules, it favors a 90° superexchange interaction, leading to ferromagnetic ordering. Once the ferromagnetic ordering becomes stable through the $Ce4f_{xyz}$–O2p–$Ce4f_{xyz}$ superexchange interaction, in heavy-doping cases the increasing numbers of electrons remaining on the oxygen vacancy sites are in turn polarized by the spin moment of neighboring Ce^{3+} ions under the ferromagnetic ordering [12].

The F-center exchange model also belongs to this category. FM in CeO_{2-y} nanocrystals is commonly explained as oxygen vacancy driven long range spin ordering, where each oxygen vacancy site, especially at the surface of nanoparticles, traps an electron forming an F center. It has been also suggested that single charged F centers are most likely essential to mediate the magnetic coupling [13].

(ii) The band ferromagnetism approach, where the magnetic moment is delocalized through the solid, and the exchange interaction I (Stoner integral) splits the majority and minority sub-bands. This method has been used by several authors [14–16] to study the ferromagnetism in CeO_2 oxides. Coey *et al* recently developed the charge-transfer model, which involves a spin-split defect band populated by charge transfer from a proximate charge reservoir. The charge-transfer ferromagnetism is of a percolating Stoner type, rather than a percolating Heisenberg type. In addition, according to the band structure calculations using density functional theory [12–15, 17, 18] it is found that spin-polarized charge density around vacancy sites leads to an electronic structure with an energy minimum for the global ferromagnetic state. Our finding [19] about electron delocalization in highly oxygen deficient $Ce(Fe^{2+}/Fe^{3+})O_{2-y}$ samples favors such an assumption and indicates that the ferromagnetism in nanooxides can be due to the electronic structure change that takes place on the nanoscale. In fact, due to the structural disorder (oxygen or cerium nonstoichiometry) a defect-related band is formed in the energy gap of CeO_{2-y} (like the impurity band in semiconductors). The density of states of the defect-related band increases with oxygen deficiency (vacancy concentration) increase and/or Fe^{3+} doping. This means that d states of iron are hybridized with Ce 4f states and the Fe^{3+} ions act as a charge reservoir. Our Raman scattering measurements clearly showed that Ce 4f electrons are in part delocalized on Ce(Fe)–O(V_0)–Ce(Fe) orbitals. It is important to note that for the d^5 electron of the Fe^{3+} ion, according to our Raman spectra, it is energetically more favorable to be transferred to the defect-related band than to be localized on the Fe ion. The existence of a high density of states at the narrow defect-related band is a necessary condition for the appearance of the room temperature ferromagnetism. Taking the Stoner integral I for oxygen as being about 1 eV [16], the obtained value $N(0) = 22\ (\text{eV})^{-1}$ from electron-molecular vibration coupling [19] is high enough to satisfy the Stoner criterion $N(0)I \geq 1$ for the appearance of ferromagnetism in nanoceria.

As far as we know, there are no experimental reports about the superparamagnetic behavior of nanoceria doped with any 3d elements. In this paper we have measured the magnetization of $Ce(Fe^{2+}/Fe^{3+})O_{2-y}$ samples as a function of temperature and magnetic field. Superparamagnetic behavior of this system is revealed by nearly zero coercive field, an appearance of the blocking temperature below 20 K, as well as the $M(H)$ dependence, which is well fitted by a weighted Langevin function which takes into account particle magnetic moment distribution.

2. Experimental details

The self-propagating-room-temperature synthesis method was used to produce high quality $Ce_{1-x}Fe_x^{2+}(Fe_x^{3+})O_{2-y}$ nanocrystals. Starting materials were metal nitrates and sodium hydroxide. The details of the sample preparation procedure can be found in our recent publications [20, 21]. The particle size of the samples under consideration, according to the x-ray diffraction (XRD) and Raman scattering measurements, was less than 5 nm [19]. Atomic force microscope (AFM) images were taken at room temperature using an Omicron B002645 SPM system, operating in non-contact mode to achieve minimal tip–sample interaction. The magnetic properties of the samples were measured in the temperature range between 75 and 300 K using a 14 T cryogen free measurement system (Cryogenic, Ltd) with a vibrating sample magnetometer VSM 2000.

3. Results and discussion

The particle size distribution (PSD) of a Fe^{3+} doped sample, derived from the AFM image (inset) is presented in figure 2. The AFM image shows that the particle diameter distribution corresponds to the log-normal profile with a maximum centered at about 10 nm. The difference between XRD and AFM sizes originates from the fact that the sizes obtained by the XRD method reflect the average size of individual nanocrystallites, whereas the sizes obtained from AFM images reflects the particle sizes which are influenced by agglomeration of nanocrystallites.

The room temperature magnetization curves as a function of magnetic field of CeO_2 poly- and CeO_{2-y} nanocrystalline samples, as well as Fe-doped $Ce_{0.88}Fe_{0.12}^{2+}(Fe_{0.12}^{3+})O_{2-y}$ nanocrystals are given in figure 3(a). These samples are diamagnetic, ferromagnetic and superparamagnetic, respectively with a significant diamagnetic (undoped samples, see the inset A in figure 3(a)) and paramagnetic contribution (Fe-doped samples). In figure 3(b) is given a reduced magnetization M_R for these samples obtained by subtracting

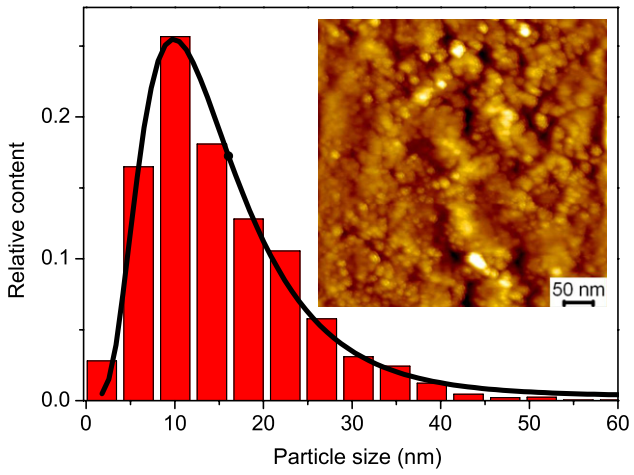

Figure 2. The particle size distribution (PSD) of the Fe^{3+} doped sample, derived from the AFM image given in the inset. The solid line represents the PSD curve calculated using the log-normal distribution with the best fit parameters: median $\mu_0 = 13.3$ nm and distribution width $\sigma = 0.55$.

the linear diamagnetic contribution for undoped CeO_2 samples (the inset B in figure 3(b)) and the linear paramagnetic contribution (represented by the lines in figure 3(a)) for Fe-doped samples. As can be seen from inset B in figure 3(b), the polycrystalline CeO_2 exhibits the expected diamagnetic behavior of closed Ce^{4+} shells, whereas the nanocrystalline CeO_{2-y} shows a small ferromagnetic contribution of about 6×10^{-3} emu g^{-1}, comparable with previous findings [22].

Figure 4 shows the magnetization of the $Ce_{0.88}Fe^{3+}_{0.12}O_{2-y}$ sample (the hysteresis loop) measured in the magnetic field up to 10 T and in the temperature range between 75 and 300 K. The reduced magnetization M_R of the same sample, obtained by subtraction of the linear paramagnetic contribution, is shown in the left inset of figure 4. The right inset presents the susceptibility of the paramagnetic contribution versus temperature of the same sample together with the Curie law calculated curve, which perfectly fits the experimental data. The magnetization curves show very low coercivity and almost linear increase of saturation magnetization with the lowering of the temperature in the measured temperature range.

The strong paramagnetic contribution in $M(H)$ dependence leads us to conclude that our samples are far from the simple assumption of single domain particles with perfect magnetic ordering. Accordingly, in figure 1 we schematically represent our sample as an assembly of core–shell particles, the magnetic behavior of which differs at the surface (mostly paramagnetic) from that of the core (mostly superparamagnetic).

The field dependence of the magnetization in the superparamagnetic materials can be described with [23]:

$$\frac{M}{M_S} = \coth\left(\frac{\mu H}{k_B T}\right) - \frac{k_B T}{\mu H} = L\left(\frac{\mu H}{k_B T}\right), \qquad (1)$$

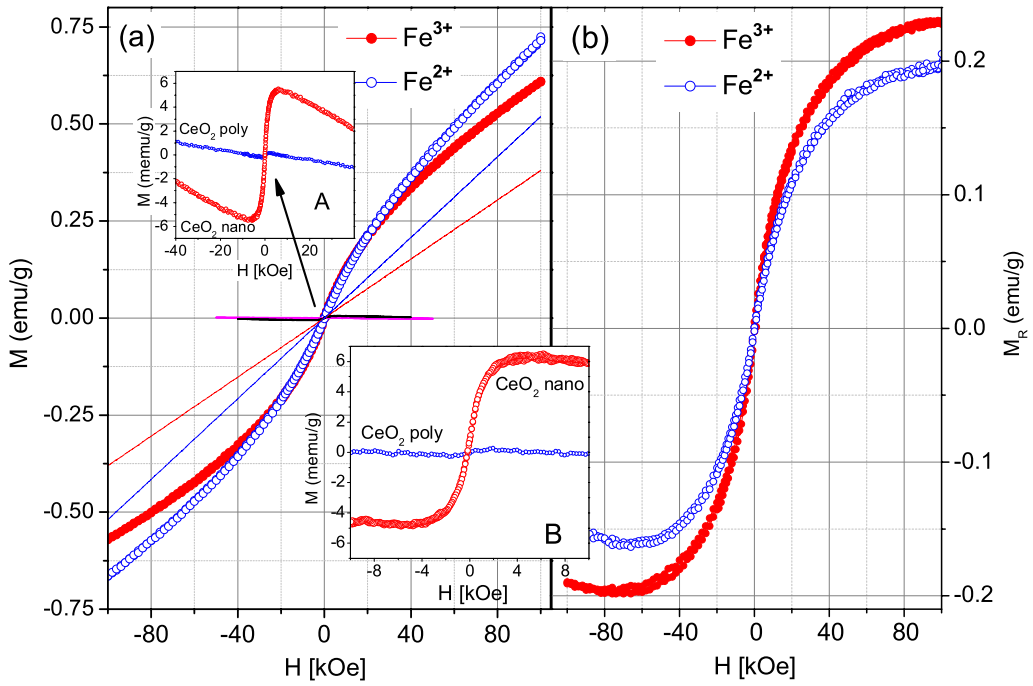

Figure 3. Magnetic properties of pure and iron-doped CeO_{2-y} nanocrystals. (a) Room temperature magnetization (M) versus magnetic field (H) curves of $Ce_{0.88}Fe^{2+}_{0.12}(Fe^{3+}_{0.12})O_{2-y}$ samples. Inset A: room temperature $M(H)$ dependence of undoped CeO_2 samples. (b) Reduced magnetization M_R of Fe-doped samples obtained by subtracting the linear paramagnetic contribution from the magnetization curves shown in (a). Inset B: reduced magnetization M_R of undoped CeO_2 samples obtained by subtracting the linear diamagnetic contribution from the magnetization curves shown in inset A.

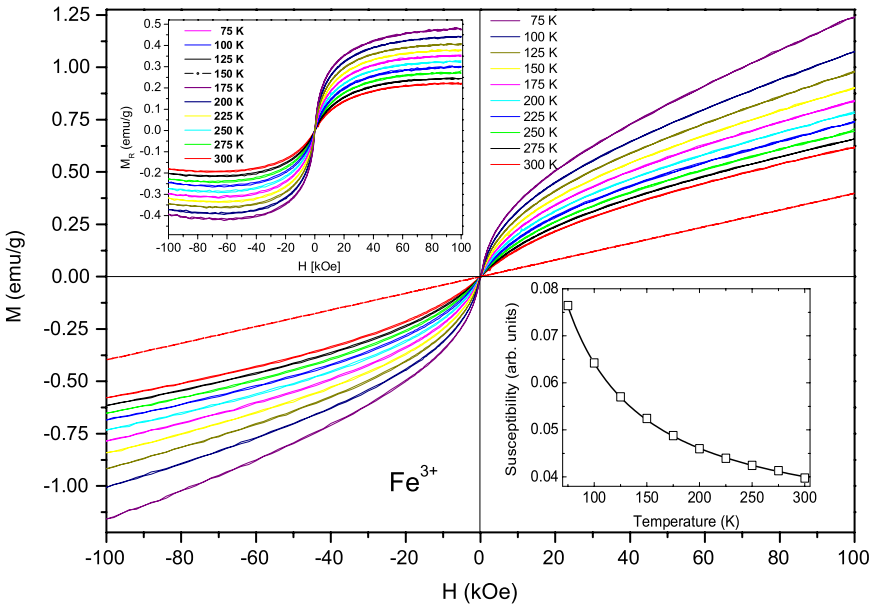

Figure 4. (a) Magnetization versus magnetic field curves of the $Ce_{0.88}Fe^{3+}_{0.12}O_{2-y}$ sample measured at different temperatures. Inset left: reduced magnetization M_R for the same sample obtained by subtracting the linear paramagnetic contributions. Inset right: susceptibility of the paramagnetic contribution versus temperature for the same sample. The solid line represents the Curie law.

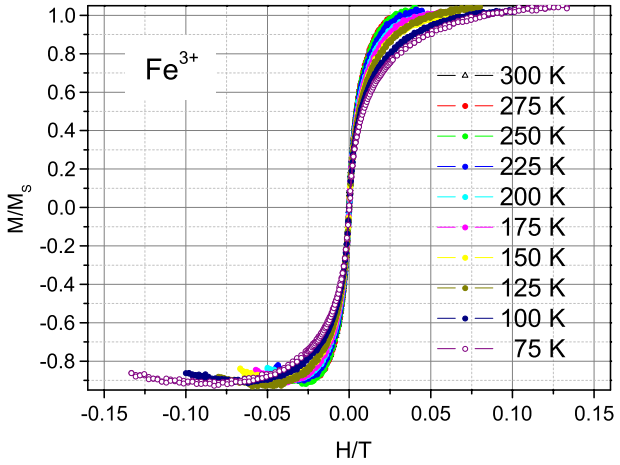

Figure 5. M/M_R versus H/T dependence (Langevin curves) at different temperatures for the $Ce_{0.88}Fe^{3+}_{0.12}O_{2-y}$ sample.

where L is the Langevin function, M_S the saturation magnetization, k_B the Boltzmann constant and μ the magnetic moment of the particles. In figure 5 we have shown the M/M_S versus H/T dependence. In an ideal superparamagnetic system, one expects that all M/M_S versus H/T curves collapse into a single universal Langevin's curve, if the measurement temperature is above the irreversibility temperature. In real nanosystems such as the case of $Ce(Fe^{2+}/Fe^{3+})O_{2-y}$ samples, there is significant deviation from the Langevin curve, particularly at lower temperatures, due to some of the following reasons: the existence of a distribution of particle sizes, random anisotropy axis distribution, surface anisotropy or interparticle magnetic interaction.

In a real nanocrystalline system the size of the particles is usually not uniform and most frequently it is described with a log-normal distribution. This kind of particle size distribution has already been used for the characterization of our samples [24]. The particle size distribution reflects in the corresponding particle moment distribution $f(\mu)$. For a real nanocrystalline system, the macroscopic magnetization can be obtained using [23]:

$$M(H,T) = \int_0^\infty \mu L\left(\frac{\mu H}{k_B T}\right) f(\mu)\,\mathrm{d}\mu \qquad (2)$$

where $f(\mu)$ is a log-normal distribution function of the type

$$f(\mu) = \frac{1}{\sqrt{2\pi}\sigma\mu}\exp\left[-\frac{\ln^2(\mu/\mu_0)}{2\sigma^2}\right], \qquad (3)$$

where σ is the distribution width and μ_0 is the median of the distribution which is related to the mean magnetic moment μ_m as $\mu_m = \mu_0 \exp(\sigma^2/2)$. In this way, the median μ_0 and the distribution width σ can be obtained through appropriate fits of the experimental magnetization curve, which is illustrated in figure 6. As can be seen from figure 6, good agreement between fits and experimental data is obtained by taking into account the log-normal magnetic moment distribution (equation (3)). Best fit parameters are given in table 1. It can be seen from table 1 that with temperature decrease, the median of the distribution decreases whereas the distribution width slightly increases. This discrepancy from the usual superparamagnetic behavior, where no temperature dependence of the distribution is expected, can be a consequence of a very wide particle size distribution. In such a case, a portion of particles will not be in the superparamagnetic but in ferromagnetic state. In that way, the apparent change in distribution will actually be a consequence of deformation of the supermagnetic curves by the presence of a small ferromagnetic component.

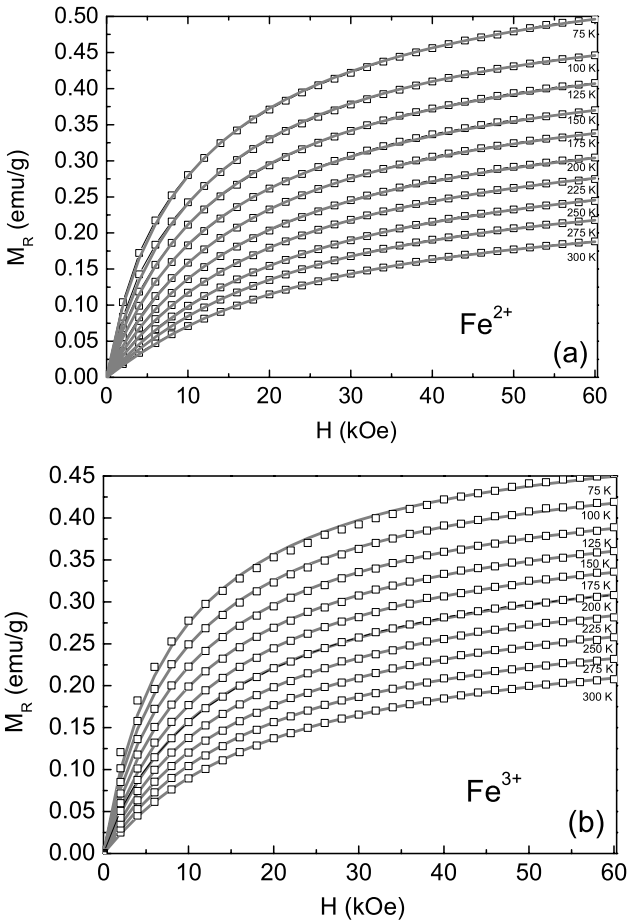

Figure 6. Magnetization versus magnetic field curves of $Ce_{0.88}Fe^{2+}_{0.12}O_{2-y}$ (a) and $Ce_{0.88}Fe^{3+}_{0.12}O_{2-y}$ (b) samples measured at different temperatures (symbols) together with $M(H)$ curves calculated using equation (2).

Table 1. Magnetic moment distribution parameters.

	Fe^{2+}		Fe^{3+}	
Temperature (K)	μ_0	σ	μ_0	σ
300	178	0.78	159	0.94
275	154	0.82	159	0.94
250	152	0.82	138	0.99
225	150	0.83	130	1.02
200	145	0.84	119	1.05
175	144	0.83	125	1.01
150	121	0.90	107	1.06
125	104	0.93	95	1.08
100	96	0.92	83	1.09
75	58	1.05	81	1.00

Figure 7 shows the low temperature dependence of the magnetization measured in zero field cooled (ZFC) and field cooled (FC) regimes in a magnetic field of 150 Oe. It can be seen that the bifurcation between ZFC and FC curves occurs at the irreversibility temperature $T_{irr} \sim 35$ K. On the other hand, the ZFC curve does not show the usual maximum which would correspond to the blocking temperature T_B, but exhibits a flatter plateau instead. This is because of the

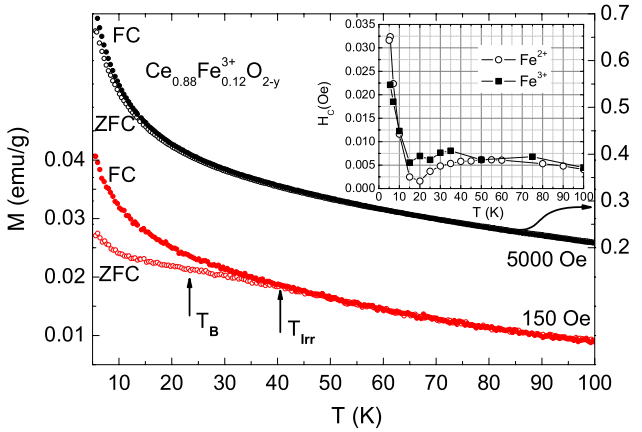

Figure 7. ZFC and FC magnetization versus temperature curves of the $Ce_{0.88}Fe^{3+}_{0.12}O_{2-y}$ sample. Inset: coercive field versus temperature dependence of $Ce_{0.88}Fe^{2+}_{0.12}$ $(Fe^{3+}_{0.12})O_{2-y}$ samples.

strong paramagnetic contribution that is superimposed on the ZFC/FC curves, and which becomes dominant at lower temperatures, effectively rising and deforming ZFC and FC curves. In an assembly of superparamagnetic particles with wide size distribution as in our case, it can be expected that the blocking temperature T_B is 2–3 times lower than T_{irr}. ZFC and FC curves in the magnetic field of 5000 Oe are also presented in figure 7. The increase in magnetic field intensity leads to the merging of ZFC and FC curves as is expected for a superparamagnetic system. The inset in figure 7 shows the coercive field for $Fe^{2+/3+}$ doped CeO_2 samples measured at different temperatures. The coercive field H_C rises abruptly below about 20 K, which represents the value of blocking temperature T_B. The appearance of a local minimum at about the blocking temperature in the $H(T)$ dependence (inset in figure 7) has already been observed in a nanocrystalline Cu–Co system [25]. Such a temperature dependence can be explained as a consequence of the temperature dependence of the average blocking temperature and the superparamagnetic susceptibility of the unblocked particles [23].

In summary, we reported magnetization measurements of $Ce_{0.88}(Fe^{2+}_{0.12}/Fe^{3+}_{0.12})O_{2-y}$ nanocrystals at various temperatures and magnetic fields. Nearly zero coercive field, the existence of the blocking temperature at about 20 K, as well as the $M(H)$ dependence, which can be fitted by a weighted Langevin function that takes into account the particle magnetic moment distribution, have led us to the conclusion that Fe-doped ceria shows superparamagnetic behavior.

Acknowledgments

This work was financially supported by the Serbian Ministry of Education and Science under the projects ON171032, III45018, and SCOPES IZ730-128169. We thank Dr B Matovic for the samples and Mr M Radovic for AFM measurements.

References

[1] Herzer G 1997 *Nanocrystalline Soft Magnetic Alloys, Handbook of Magnetic Materials* vol 10, ed K H J Buschow (Amsterdam: Elsevier Science) chapter 3, p 418

[2] Stoner E C and Wohlfarth E P 1948 *Phil. Trans. R. Soc.* A **240** 599
Reprinted by Stoner E C and Wohlfarth E P 1991 *IEEE Trans. Magn.* **27** 3475
Tannous C and Gieraltowski J 2008 *Eur. J. Phys.* **29** 475

[3] Kodama R H, Makhlouf S A and Berkowitz A E 1997 *Phys. Rev. Lett.* **79** 1393

[4] He W D, Somarajan S, Koktysh D S and Dickerson J H 2011 *Nanscale* **3** 184

[5] He W D, Osmulski M E, Lin J H, Koktysh D S, McBride J R, Park J H and Dickerson J H 2012 *J. Mater. Chem.* **22** 16728

[6] Sundaresan A and Rao C N R 2009 *Nano Today* **4** 94

[7] Fernandes V, Schio P, de Oliveira A J A, Schreiner W H, Varalda J and Mosca D H 2011 *J. Appl. Phys.* **110** 113002 and references therein

[8] Dohčević-Mitrović Z D, Paunović N, Radović M, Popović Z V, Matović B, Cekić B and Ivanovski V 2010 *Appl. Phys. Lett.* **96** 203104

[9] Li G R, Qu D L, Arurault L and Tong Y 2009 *J. Phys. Chem.* C **113** 1235

[10] Dimri M C, Khanduri H, Kooskora H, Subbi J, Heinmaa I, Mere A, Krustok J and Stern R 2012 *Phys. Status Solidi* a **209** 353

[11] Paunović N, Dohčević-Mitrović Z D, Scurtu R, Aškrabić S, Prekajski M, Matović B and Popović Z V 2012 *Nanoscale* **4** 5469

[12] Han X, Lee J and Yoo H I 2009 *Phys. Rev.* B **79** 100403

[13] Shah L R, Ali B, Zhu H, Wang W G, Song Y Q, Zhang H W, Shah S I and Xiao J Q 2009 *J. Phys.: Condens. Matter* **21** 486004

[14] Ge M Y, Wang H, Liu E Z, Liang J Z, Li Y K, Xu Z A and Li H Y 2008 *Appl. Phys. Lett.* **93** 062505

[15] Fernandes V *et al* 2009 *Phys. Rev.* B **80** 035202

[16] Coey J M D, Wongsaprom K, Alaria J and Venkatesan M 2008 *J. Phys. D: Appl. Phys.* **41** 134012
Coey J M D, Stamenov P, Gunning R D, Venkatesan M and Paul K 2010 *New J. Phys.* **12** 050325

[17] Fernandes V *et al* 2010 *J. Phys.: Condens. Matter* **22** 216004

[18] Castleton W M, Kullgren J and Hermansson K 2007 *J. Chem. Phys.* **127** 244704

[19] Popović Z V, Dohčević-Mitrović Z D, Paunović N and Radović M 2012 *Phys. Rev.* B **85** 014302

[20] Radović M, Dohčević-Mitrović Z D, Paunović N, Šćepanović M, Matović B and Popović Z V 2009 *Acta Phys. Pol.* A **116** 84

[21] Matović B, Dohčević-Mitrović Z, Radović M, Branković Z, Branković G, Bošković S and Popović Z V 2009 *J. Power Sources* **193** 146

[22] Wen Q-Y, Zhang H-W, Song Y-Q, Yang Q-H, Zhu H and Xiao J Q 2007 *J. Phys.: Condens. Matter* **19** 246205

[23] Knobel M, Nunes W C, Socolovsky L M, De Biasi E, Vargas J M and Denardin J C 2008 *J. Nanosci. Nanotechnol.* **8** 2836

[24] Aškrabić S, Dohčević-Mitrović Z D, Kremenović A, Lazarević N, Kahlenberg V and Popović Z V 2012 *J. Raman Spectrosc.* **43** 76

[25] Nunes W C, Folly W S D, Sinnecker J P and Novak M A 2004 *Phys. Rev.* B **70** 014419